Constellation Design for a Multicarrier Optical Wireless Communication Channel

Qian Gao, *Member, IEEE*, Jonathan H. Manton, *Senior Member, IEEE*,
Gang Chen, *Member, IEEE*, and Yingbo Hua, *Fellow, IEEE*

***Abstract*—A block-wise constellation design is presented for optical communication systems with multi-subcarrier modulation (MSM), intensity modulation (IM) and direct detection (DD). The DC-bias traditionally used only for compensating the negative peaks of the transmitter-side signals is treated as an information-carrying basis in our proposed scheme called MSM-JDCM. Designs are done for both flat-fading and frequency selective-fading scenarios, and following a principle of high dimensional sphere packing. To simplify the problem, we apply the following methods. First, we use bounds on the waveform's maximum and minimum. Second, we use the maximum and minimum constraints on a set of sufficient samples of waveforms. Third, we relax non-convex distance constraints into convex ones by iterative linearizations. With the MSM-JDCM, we minimize electrical power, optical power, and peak power with a common target bit error rate (BER). Analysis shows that the MSM-JDCM offers significant power gains over MSM-Normal and MSM-SPSS. The short-term peak to average power ratio (PAPR) and long-term PAPR constraints are combined with the MSM-JDCM to mitigate the nonlinear distortion caused by high power amplifier and laser diode, which is another novelty of our scheme. To attain lower BER, a binary switching algorithm (BSA) is applied to find the improved constellation labeling.**

***Index Terms*—Optical wireless communication, constellation design, multicarrier optical, IM/DD, frequency-selective optical channels, peak to average power ratio, constellation labeling/mapping.**

I. Introduction

In recent decades, there has been an increasing level of interests in optical wireless communications, including infrared, visible light, and ultraviolet communications [1]–[4]. Optical wireless communications offer a potential of high-speed transmissions in unregulated bands. Analogous to the multicarrier modulation employed in the RF systems [5], multiple-subcarrier modulation (MSM) has been proposed for the optical systems [6]–[9], where a transmitter modulates multiple electrical subcarriers onto the optical carrier through intensity modulation (IM), and a receiver captures the intensity modulated signals by a way of direct detection (DD). This is a non-coherent system and much cheaper to implement than its counterparts known as the all-optical systems [10].

Manuscript received March 1, 2013; revised August 20 and November 5, 2013. The editor coordinating the review of this paper and approving it for publication was E. Agrell.

Q. Gao, G. Chen, and Y. Hua are with the Department of Electrical Engineering, University of California, Riverside, CA 92521, USA (e-mail: {qgao, gachen, yhua}@ee.ucr.edu).

J. H. Manton is with the Department of Electrical and Electronic Engineering, The University of Melbourne, Parkville, Australia (e-mail: j.manton@ee.mu.oz.au).

Digital Object Identifier 10.1109/TCOMM.2013.112213.130166

MSM along with IM/DD is a widely considered scheme for use in scattering environments [11]–[13]. For flat-fading environment, MSM is known to yield a higher spectral efficiency than traditional binary modulation techniques such as on-off keying (OOK) and pulse position modulation (PPM) [14, Chapter 5]. However, to our knowledge, MSM has been used only for flat-fading channels.

Constellation design is important for MSM IM/DD systems [15]–[17]. A good constellation design should be power efficient, including electrical, optical and peak-power efficiencies. A stream-wise scheme termed MSM-Normal is proposed in [15], and a block-wise one termed MSM-SSPS (subcarrier signal point sequence) is in [16] and [17]. With the MSM-Normal, bit sequences are independently modulated onto individual subcarriers using BPSK/QPSK (binary phase shift keying and quadrature phase shift keying). But the sum of the subcarrier waveforms likely contains a large negative peak which needs to be compensated by a DC (direct current) power, which compromises the power efficiency. With the MSM-SSPS, a more general constellation for multiple subcarriers with both I and Q channels is designed, which requires a less DC power for negative peak compensation. However, none of these two schemes treats the DC-bias as part of the information basis. In [18], a sphere packing problem is formulated for constellation design of a single-carrier system, which treats the DC-bias as an information carrying basis.

In this paper, we will consider the constellation design for the MSM IM/DD system with either flat fading or frequency-selective fading channels. We propose a joint DC and multicarrier constellation design scheme, termed MSM-JDCM. This scheme provides an optimized constellation in a connected region in high dimensional space with the DC-bias as an information basis. Convex optimization problems are formulated in Section III and solved by CVX [20] to provide optimized constellations. A good constellation design should not only be power efficient but also robust to the HPA and/or LD's nonlinearities. To deal with these nonlinearities, traditional schemes include selective mapping [21], partial transmit sequence [22], clipping [23], tone reservation [24], vector precoding [25], companding transform [26], and others [27]. In this paper, we show that our constellation design scheme MSM-JDCM, along with short-term PAPR (peak to average power ratio) or long-term PAPR constraints, provides a robustness against the nonlinearities. Near the end of the paper, we also consider a labeling problem (i.e., bits-to-symbols mapping) after a constellation is given. In the literature, the

labeling schemes include the Gray Code mapping [28], set-partitioning mapping [29], [30], maximum squared Euclidean weight mapping [31], the binary switching algorithm (BSA) [32]. Among them, the BSA is able to accommodate labeling in a high dimensional space, and our simulation results show that the labeling using BSA noticeably reduces the BER (bit error rate) for a fixed SER (symbol error rate). A brief version of this paper is available in [19].

Throughout the paper, we will use the following conventions. Boldface upper-case letters denote matrices, boldface lower-case letters denote column vectors, and standard lower-case letters denote scalars. $(\cdot)^T$ and $(\cdot)^{-1}$ denote the transpose and inverse operators. $*$ denotes convolution. $\mathcal{E}$ denotes the expectation operator. $< \cdot >$ and $|| \cdot ||$ denote the Euclidean inner product and Euclidean norm. $\otimes$ denotes the Kronecker product. $\mathcal{R}^n$ denotes the n-dimensional real space. The set of all integers is denoted by $\mathbb{Z}$. By $\mathbf{e}_i$, we denote a vector with all zeros but the value one at the i-th element. By $\mathbf{I}$, we denote the identity matrix. By $\mathbf{O}$, we denote an all zero matrix. And $\nabla(\cdot)$ denotes the gradient operator.

II. MSM IM/DD OPTICAL COMMUNICATION SYSTEMS

A. The Flat-fading Channel Model

Fig. 1 shows the system block diagram of an IM/DD optical wireless network. The received signal $y(t)$ can be written as [2]

$$y(t) = \gamma\eta s(t) * h(t) + v(t) \tag{1}$$

where t is continuous time index, $s(t)$ denotes the intensity signal sent by the laser diode (LD), $y(t)$ the received photocurrent by the photodetector (PD), $h(t)$ the channel impulse response, η the electro-optical conversion factor in watts per ampere (W/A), and γ the photodetector responsivity. Signal intensity has to be non-negative, i.e.,

$$s(t) \geq 0 \tag{2}$$

which is the fundamental constraint differentiating IM/DD from many coherent modulated systems and an important basis of the schemes mentioned later in this article.

The proposed methods for constellation design and labeling require the channel state information which is typically static and easy to obtain for practical indoor optical wireless communications. We consider flat-fading channel model first. With a constant channel $h = 1$ assumed for multiple symbol intervals, the model is simplified to

$$r(t) = \gamma\eta s(t) + n(t) \tag{3}$$

where $\gamma\eta = 1$ can be further assumed without loss of generality. In our design, $s(t)$ is chosen from a signal set $\mathcal{S} = \{s_1(t), s_2(t), \ldots, s_{N_c}(t)\}$, where each signal in the set is to be designed and N_c is the constellation size. The discrete vector channel model can be written as:

$$\mathbf{r}[p] = \mathbf{s}[p] + \mathbf{n}[p] \qquad p \in [1, N_c] \tag{4}$$

where we assume the noise vector $\mathbf{n}[p]$ has independent random Gaussian elements with zero mean and variance $N_0/2$ per dimension. We refer the readers to [18] for details about the relationship between the discrete and continuous channel

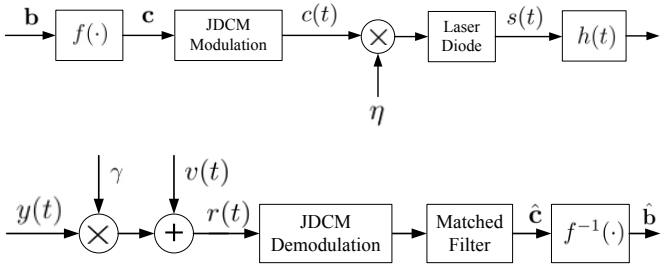

Fig. 1. The system block diagram with the MSM-JDCM.

models. It should be noted that $[p]$ is to index the "discrete" signal space and (t_n) will be used to index the "discrete" time samples of the continuous signal waveforms.

Power metrics are thus defined: 1. the average electrical power $\Psi_e(t) = \frac{1}{T_s}\mathcal{E}_i[s_i^2(t)]$ (the average is taken over i); 2. the average optical power $\Psi_o(t) = \frac{\eta}{\sqrt{T_s}}\mathcal{E}_i[s_i(t)]$, 3. the peak optical power $\Psi_{po}(t) = \eta \max_{i,t} s_i(t)$. The index i is uniformly taking value from set $\mathcal{I} = \{1, 2, \ldots, N_c\}$ and T_s is the symbol interval. The peak electrical power $\Psi_{pe}(t)$ is optimal as long as $\Psi_{po}(t)$ is optimized [18] so that it is omitted here. Other metrics such as the PAPR and dynamic range are analyzed in Section IV.

B. The information basis

Our transmission scheme is illustrated in Fig. 1. Denote $\boldsymbol{\phi}(t) = [\phi_1(t), \phi_2(t), \ldots, \phi_M(t)]^T$ as a sequence of orthonormal information basis modulated by $\mathbf{c}_i$, the i-th symbol vector. $\phi_1(t)$ is associated with the DC-bias, which is as well used by MSM-Normal and MSM-SSPS, but only for biasing purpose (not an information basis and is dropped by the receiver). The transmitted signal $s_i(t)$ by the LD is given by $s_i(t) = \eta\boldsymbol{\phi}^T(t)\mathbf{c}_i$.

If both I and Q channels are used by each subcarrier for MSM-JDCM, we term it MSM-JDCM-IQ, thus $M = 2K+1$. If only the I channels are used, we term it MSM-JDCM-I, thus $M = K + 1$. The information basis is typically chosen as follows.

$$\phi_1(t) = \sqrt{\frac{1}{T_s}}\Pi(\frac{t}{T_s}) \tag{5}$$

$$\phi_{2k}(t) = \sqrt{\frac{2}{T_s}}\cos(2\pi f_k t)\Pi(\frac{t}{T_s}) \qquad k = 1, 2, \ldots, K \tag{6}$$

$$\phi_{2k+1}(t) = \sqrt{\frac{2}{T_s}}\sin(2\pi f_k t)\Pi(\frac{t}{T_s}) \qquad k = 1, 2, \ldots, K \tag{7}$$

where

$$\Pi(t) = \begin{cases} 1, & \text{if } 0 \leq t < 1 \\ 0, & \text{otherwise.} \end{cases} \tag{8}$$

where $f_k = \frac{k}{T_s}$ is the frequency of k-th subcarrier. The rectangular window defined in (8) is not a practical signal to use in a real-world IM/DD channel due to its infinite bandwidth requirement, thus in this paper we propose to employ a "time-domain raised cosine (TDRC)" window defined as follows

$$\tilde{\Pi}(t) = \begin{cases} 0.5\big(1 + \cos[\frac{\pi}{\beta}(t - \beta)]\big) & \text{if} \quad 0 < t < \beta, \\ 1 & \text{if} \quad \beta \leq t \leq 1 - \beta, \\ 0.5\big(1 + \cos[\frac{\pi}{\beta}(t - 1 + \beta)]\big) & \text{if} \quad 1 - \beta < t \leq 1. \end{cases} \tag{9}$$

We will choose a small β in this paper.

C. The waveform distances

The basis waveforms are typically normalized, i.e., the following holds

$$< \phi_n(t), \phi_m(t) >= \begin{cases} 1 & m = n, \\ 0 & \text{otherwise.} \end{cases} \tag{10}$$

Straightforwardly, the inner product and Euclidean distance relationships between two waveforms hold as follows

$$< c_i(t), c_j(t) >=< \mathbf{c}_i, \mathbf{c}_j > \tag{11}$$

$$||c_i(t) - c_j(t))|| = ||\mathbf{c}_i - \mathbf{c}_j|| \tag{12}$$

The detection performance at the receiver, especially at high signal-to-noise ratio (SNR), is governed by the minimum distance among all waveform pairs.

D. The bit-to-symbol mapping

For the MSM-JDCM and MSM-SPSS, the bit sequence $\mathbf{b}_i$ is mapped onto a symbol vector $\mathbf{c}_i$ jointly, i.e.,

$$\mathbf{c}_i = f(\mathbf{b}_i) \tag{13}$$

where $\mathbf{b}_i \in \{\mathbf{b}_1, \mathbf{b}_2, \ldots, \mathbf{b}_{N_c}\} \in \mathcal{R}^{N_b}$, $\mathbf{c}_i \in \{\mathbf{c}_1, \mathbf{c}_2, \ldots, \mathbf{c}_{N_c}\} \in \mathcal{R}^M$, and $N_c = 2^{N_b}$. $f(\cdot)$ is called the "block-wise (BLW)" mapping function.

For the MSM-Normal, "subcarrier-wise (SCW)" mapping is employed, which maps bits onto subcarriers individually, i.e.

$$(c_{I,k}, c_{Q,k}) = \tilde{f}(b_{I,k}, b_{Q,k}) \qquad k = 1, \ldots, K \tag{14}$$

where I and Q stand for real and imaginary part respectively. $(c_{I,k}, c_{Q,k})$ can take values from only $(\pm a, \pm a)$. The summation of all subcarriers pulses is then biased. The designing of the mapping functions is referred to as "constellation labeling" problem.

E. MSM-JDCM vs MSM-SSPS

The advantage of the MSM-JDCM over the MSM-SSPS is threefold: 1. the dimension of information basis of the MSM-JDCM is always higher than the MSM-SSPS by one, which is due to the use of DC-bias as information basis; 2. the MSM-JDCM searches constellation points in a continuous space, while MSM-SSPS restricts the searching space to a "discrete lattice" of size 9^K. Each subcarrier picks symbols from a (8+1)-APSK constellation [17]; 3. MSM-SPSS has to use both I and Q channels for each subcarrier.

F. The selective-fading channel model

While multiple non-line-of-sight optical links exist, we choose the geometric series model for analysis in the paper, i.e.,

$$h'(t) = \gamma \sum_i \beta_i \delta(t - \tau_i) \tag{15}$$

where $\delta(\cdot)$ is a dirac-delta function, $0 < \beta_i < 1$ and $\tau_i \ll T_s$ are real numbers denoting the gain and delay of the i-th channel tap respectively. γ is a very small value denoting the common path-loss which can be lumped into noise variance, and therefore we only consider the simplified channel

$$h(t) = \sum_i \beta_i \delta(t - \tau_i) \tag{16}$$

There are other choices for modeling the selective-fading channel, e.g., the exponential decay model, ceiling bounce model, and etc.. Comparisons among different channel models can be found in [36]. With the chosen $h(t)$, we propose to design a set of pre-equalizers before $\mathbf{c}_i$ comes into the JDCM modulator.

Proposition 1. *The pre-equalizers that mitigate the effect of frequency-selective channel* (16) *are linear, and have the following form:*

$$\mathbf{P}_k = \frac{1}{|z_k|^2} \begin{bmatrix} Re(z_k) & -Im(z_k) \\ Im(z_k) & Re(z_k) \end{bmatrix}, \qquad \textit{for k-th subcarrier}$$

$$p_o = \frac{1}{\sum_i \beta_i}, \qquad \textit{for DC-bias}$$

where $z_k = \sum_i \beta_i e^{-k2\pi f_k \tau_i}$. *Thus the modulating vector* $\tilde{\mathbf{c}}_i = \mathbf{P}\mathbf{c}_i$, *where the symbol vector* $\mathbf{c}_i$ *is pre-equalized by the block-diagonal matrix* $\mathbf{P} = \textbf{\textit{bdiag}}\{p_0, \mathbf{P}_1, \ldots, \mathbf{P}_K\}$.

The proof can be found in Appendix B.

III. The Optimization Problem

A. The objective functions

The MSM-JDCM is targeted at optimizing the joint symbol vector $\mathbf{c_T} = [\mathbf{c}_1^T, \mathbf{c}_2^T, \ldots, \mathbf{c}_{N_c}^T]^T \in \mathcal{R}^{(2K+1)N_c}$ (for the IQ channels case). When the optimization goal is to minimize the average electrical power, the objective function is given by

$$\Psi_e(\mathbf{c_T}) = \frac{1}{N_c T_s} \sum_{i=1}^{N_c} ||\mathbf{c}_i||^2 = \frac{1}{N_c T_s} \mathbf{c_T}^{\boldsymbol{T}} \mathbf{c_T} \tag{17}$$

where i is uniformly distributed over $\mathcal{I}$. While for minimizing the optical average power, the objective function is written as

$$\Psi_o(\mathbf{c_T}) = \frac{\eta}{N_c \sqrt{T_s}} \sum_{i=1}^{N_c} c_{i,1} = \frac{\eta}{N_c \sqrt{T_s}} \sum_{i=1}^{N_c} \mathbf{j}_{(i-1)M+1}^T \mathbf{c_T} \tag{18}$$

where $\mathbf{j}_{(i-1)M+1} = [0, \ldots, 1, \ldots, 0]^T$ is a $(2K+1)N_c \times 1$ column vector with all zeros at except the $(i-1)M+1$'s element, and therefore only the DC-bias part of each candidate waveform is averaged. The exact form of optical peak power constraint is hard to get and we aim at the upper bound of it as in the following. For a an arbitrary packet, the optical peak

power is

$$\begin{aligned}\Psi_{po}(\mathbf{c_T}) &= \eta \max_{t,i} c_i(t - jT_s) = \eta \max_{t,i} c_i(t) \\ &\le \frac{\eta}{\sqrt{T_s}} \max_i \{\sum_{k=1}^{K} \sqrt{2(c_{i,2k}^2 + c_{i,2k+1}^2)} + c_{i,1}\} \\ &= \frac{\eta}{\sqrt{T_s}} \max_i \{\sum_{k=1}^{K} ||\mathbf{A}_k \mathbf{c}_i|| + \mathbf{a}_0^T \mathbf{c}_i\} \\ &= \frac{\eta}{\sqrt{T_s}} \max_i \{\sum_{k=1}^{K} ||\mathbf{A}_k \mathbf{J}_i \mathbf{c_T}|| + \mathbf{a}_0^T \mathbf{J}_i \mathbf{c_T}\} \\ &= \frac{\eta}{\sqrt{T_s}} \max_i \{\sum_{k=1}^{K} ||\mathbf{W}_{i,k} \mathbf{c_T}|| + \mathbf{w}_{i,0}^T \mathbf{c_T}\} \qquad (19)\end{aligned}$$

$$\Psi_{pe}(\mathbf{c_T}) = \frac{\Psi_{po}^2(\mathbf{c_T})}{\eta^2} \qquad (20)$$

(19) can be straightforwardly derived to upper bound the peak power, and we later show in III-D that this bound can be replaced by a set of point-wise constraints. By introducing the following notations: $\mathbf{A}_k = \sqrt{2}\,\mathrm{diag}(0,\ldots,0,1,1,0,\ldots,0)$ with the $2k$-th and $2k+1$-th elements as 1's, $\mathbf{a}_0 = [1,0,\ldots,0]^T$ of dimension $(2K+1)\times 1$, $\mathbf{J}_i = [\mathbf{O}_{2K+1},\ldots,I_{2K+1},\mathbf{O}_{2K+1},\ldots,\mathbf{O}_{2K+1}]$ of dimension $2K+1 \times N_c(2K+1)$, $\mathbf{W}_{i,k} \triangleq \mathbf{A}_k\mathbf{J}_i$, and $\mathbf{w}_{i,0}^T \triangleq -\mathbf{a}_0^T\mathbf{J}_i$. The optical peak power $\Psi_{po}(\boldsymbol{c})$ and electrical peak $\Psi_{pe}(\boldsymbol{c})$ power has a relationship of (20) such that optimizing one automatically guarantees the optimality of the other.

Besides the performance metrics mentioned above, one can choose to use linear combination of a number of objectives, or by running the optimization solver multiple times with more and more severe constraints. In other words, because there are competing performance metrics, there could be a range of different answers depending on which metrics are more important. This is important in practice and one can formulate different problems with combining or modifying the problems we address in this paper.

B. The constraints

With IQ channels, The symbol vector $\mathbf{c}_i \in \mathcal{R}^{2K+1}$ can take values from a connected region as long as the nonnegative constraint is satisfied as follows.

$$\min_t c_i(t) = \min_{i,t} \boldsymbol{\phi}(t)^T \mathbf{c}_i = \min_t \sum_{m=1}^{2K+1} c_{i,m}\phi_m(t) \ge 0 \qquad (21)$$

With derivations in the equation at the bottom of the page, a sufficient but not necessary set of constraints can be used to guarantee the nonnegativeness of the transmitted signals as follows

$$\begin{aligned}G_i(\mathbf{c_T}) &\triangleq c_{i,1} - \sum_{k=1}^{K} \sqrt{2(c_{i,2k}^2 + c_{i,2k+1}^2)} \\ &= \mathbf{w}_{i,0}^T \mathbf{c_T} + \sum_{k=1}^{K} ||\mathbf{W}_{i,k}\mathbf{c_T}|| \ge 0 \qquad \forall i \qquad (22)\end{aligned}$$

These are convex constraints in $\mathbf{c_T}$. Later we show in III-D that a set of point-wise constraints serves as a replacement of this bound, with very little computational redundancy.

Besides the non-negativeness of signal, constraint has to be put also on the minimum distance among all constellation point pairs.

$$h_l(\mathbf{c_T}) \triangleq {\mathbf{c_T}}^T \mathbf{F}_l \mathbf{c_T} \ge d_{min}, \qquad l = 1,2,\ldots \frac{(N_c-1)N_c}{2} \qquad (23)$$

where $\mathbf{F}_{l(p,q)} = \mathbf{E}_{pq}$, $\mathbf{E}_p = \mathbf{e}_p^T \otimes \mathbf{I}_{N_c}$, $\mathbf{e}_p$ has a dimension of $(2K+1)\times 1$, and $\mathbf{E}_{pq} = \mathbf{E}_p^T\mathbf{E}_p - \mathbf{E}_p^T\mathbf{E}_q - \mathbf{E}_q^T\mathbf{E}_p + \mathbf{E}_q^T\mathbf{E}_q$. The following relation holds.

$$l(p,q) = (p-1)N_c - \frac{p(p+1)}{2} + q, \quad p,q \in 1,2,\ldots,N_c,\ p<q \qquad (24)$$

For short, replace $l(p,q)$ with l. $d_{min} = 1$ is assumed throughout this paper without loss of generality.

The distance constraints are nonconvex in $\mathbf{c_T}$ and we firstly approximate the exteriors of the ellipses (high order cylinders) $h_l(\boldsymbol{c}) < 1$ with the first order Taylor series at ${\mathbf{c_T}}^{(0)}$, i.e.

$$\begin{aligned}h_l(\mathbf{c_T}) &\cong H_l^{(0)}(\mathbf{c_T}) \\ &= h_l({\mathbf{c_T}}^{(0)}) + \nabla h^T({\mathbf{c_T}}^{(0)})(\mathbf{c_T} - {\mathbf{c_T}}^{(0)}) \\ &= {\mathbf{c_T}}^{(0)T}\mathbf{F}_l{\mathbf{c_T}}^{(0)} + 2{\mathbf{c_T}}^{(0)T}\mathbf{F}_l(\mathbf{c_T} - {\mathbf{c_T}}^{(0)}) \\ &= 2{\mathbf{c_T}}^{(0)T}\mathbf{F}_l\mathbf{c_T} - {\mathbf{c_T}}^{(0)T}\mathbf{F}_l{\mathbf{c_T}}^{(0)} \ge 1, \qquad \forall l \qquad (25)\end{aligned}$$

This approximation restricts the feasible region into a half space defined by $H_l^{(0)}(\mathbf{c_T}) \ge 1$. By running the algorithm with the above approximation once a new point ${\mathbf{c_T}}^{(1)}$ is found, which is guaranteed to maintain $1 \le {\mathbf{c_T}}^{(1)T}\mathbf{F}_l{\mathbf{c_T}}^{(1)} \le {\mathbf{c_T}}^{(0)T}\mathbf{F}_l{\mathbf{c_T}}^{(0)}$ [33]. Then using Taylor series again at ${\mathbf{c_T}}^{(1)}$, the feasible region is now approximated by a new halfspace $H_l^{(1)}(\mathbf{c_T}) \ge 1$, which has $H_l^{(0)}(\mathbf{c_T}) \ge 1$ as a subspace. We call this process as the "iterative Taylor series approximation", which iteratively finds the supporting hyperplane of $h_l(\mathbf{c_T}) < 1$ as the feasible region containing a local optimum. With multiple runs at a set of wide spread initial points, we expect to find the global optimum.

For simplicity, we drop the iteration index and write the minimum distance constraint as:

$$1 - H_l(\mathbf{c_T}) \le 0, \qquad \forall l \qquad (26)$$

$$\begin{aligned}\min_t c_i(t) \quad &= \min_t \left[\sqrt{\tfrac{1}{T_s}} c_{i,1}\Pi(\tfrac{t}{T_s}) + \sqrt{\tfrac{2}{T_s}}\big(\textstyle\sum_{k=1}^{K} c_{i,2k}\cos(2\pi f_k t) + \sum_{k=1}^{K} c_{i,2k+1}\sin(2\pi f_k t)\big)\Pi(\tfrac{t}{T_s})\right] \\ &= \sqrt{\tfrac{1}{T_s}}\min_t \left[c_{i,1} + \textstyle\sum_{k=1}^{K}\sqrt{2(c_{i,2k}^2 + c_{i,2k+1}^2)}\cos(2\pi f_k t - \theta_k)\right] \qquad t \in [0,T_s] \\ &\ge \sqrt{\tfrac{1}{T_s}}\min_t \left[c_{i,1} - \textstyle\sum_{k=1}^{K}\sqrt{2(c_{i,2k}^2 + c_{i,2k+1}^2)}\right] \qquad t \in [0,T_s]\end{aligned}$$

C. The optimization problems

We explicitly write out the formulation with peak power minimization objective:

$$\begin{aligned} \min_{\mathbf{c_T},v} \quad & v \\ \text{s.t.} \quad & \mathbf{w}_{i,0}^T\mathbf{c_T} + ||\mathbf{W}_{i,k}\mathbf{c_T}|| \geq 0, \qquad \forall i \\ & -\mathbf{w}_{i,0}^T\mathbf{c_T} + ||\mathbf{W}_{i,k}\mathbf{c_T}|| \leq v, \qquad \forall i \\ & 1 - 2\mathbf{c_T}^{(0)T}\mathbf{F}_l\mathbf{c_T} + \mathbf{c_T}^{(0)T}\mathbf{F}_l\mathbf{c_T}^{(0)} \leq 0, \qquad \forall l \end{aligned} \tag{27}$$

The optimization is done iteratively, and the initial point $\mathbf{c_T}^{(0)}$ has to be a feasible point, i.e., satisfying the constraints $\mathbf{c_T}^{(0)T}\mathbf{F}_l\mathbf{c_T}^{(0)} \geq d_{min}$ and $\mathbf{w}_{i,0}^T\mathbf{c_T}^{(0)} + ||W_{i,k}\mathbf{c_T}^{(0)}|| \leq 0$ for all i. It is straight forward to show after each iteration, the new solution $\mathbf{c_T}^{(1)}$ will also be a feasible point and $p_1 \leq p_0$ accordingly [33]. The stopping criterion is chosen as $||p_k - p_{k+1}|| < \epsilon$, where ϵ is a small real value such as 10^{-4} (we choose different ϵ values for different goals in our simulation). Similar remarks can be made for those with criterion $\Psi_e(\mathbf{c_T})$ and $\Psi_o(\mathbf{c_T})$.

When the number of subcarriers is large, the computation of the MSM-JDCM and the MSM-SSPS grow so that regular PCs typically cannot handle the designs. We could turn to super computers with larger memory and higher processing capability, since this is just a "once-off" process.

D. The point-wise constraints

As mentioned, the upper bound of peak power (19) and lower bound of non-negative constraint (17) can be replaced by a set of point-wise constraints respectively. The reason for such replacement is that these bounds are not tight enough and a tighter bound is hard to find. By point-wise constraint, it is meant that all possible waveforms $c_i(t)$ defined in $[0, T_s]$ are sampled at a set of discrete points t_n and instead of $c_i(t)$, $c_i(t_n)$ $\forall n$ are constrained, where

$$t_n = \frac{nT_s}{N} = \frac{nT_s}{2KN_O}, \qquad n = 0, 1, \ldots, N \tag{28}$$

where N_O denotes the oversampling rate for the subcarrier with highest frequency. It is observed in our simulations that with $N_O \geq 4$, the MSM-JDCM with point-wise constraints is able to outperform its counterpart with bounds. With flat-fading channel, the peak power minimization with point-wise constraints can be written as:

$$\begin{aligned} \min_{\mathbf{c_T},v} \quad & v \\ \text{s.t.} \quad & \mathbf{u}_n^T\mathbf{J}_i\mathbf{c_T} \geq 0, \qquad \forall (i,n) \\ & \mathbf{u}_n^T\mathbf{J}_i\mathbf{c_T} \leq v, \qquad \forall (i,n) \\ & 1 - 2\mathbf{c_T}^{(0)T}\mathbf{F}_l\mathbf{c_T} + \mathbf{c_T}^{(0)T}\mathbf{F}_l\mathbf{c_T}^{(0)} \leq 0, \qquad \forall l \end{aligned} \tag{29}$$

where $\mathbf{u}_n = [u_{n,0}, u_{n,1}^c, u_{n,1}^s, \ldots, u_{n,K}^c, u_{n,K}^s]^T$, $u_{n,0} = \sqrt{1/T_s}$, $u_{n,k}^c = \sqrt{2/T_s}\cos(2\pi f_k t_n)$, and $u_{n,k}^s = \sqrt{2/T_s}\sin(2\pi f_k t_n)$. We use MSM-JDCMP as an abbreviation for MSM-JDCM with point-wise constraints to distinguish from MSM-JDCMB, which denotes the MSM-JDCM with upper or lower bounds as constraints. With selective-fading channel, $\mathbf{c_T}$ is replaced with $\mathbf{Pc_T}$ in the first two constraints.

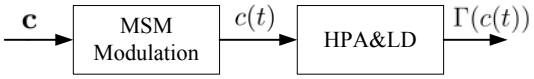

Fig. 2. System impaired by the HPA and LD.

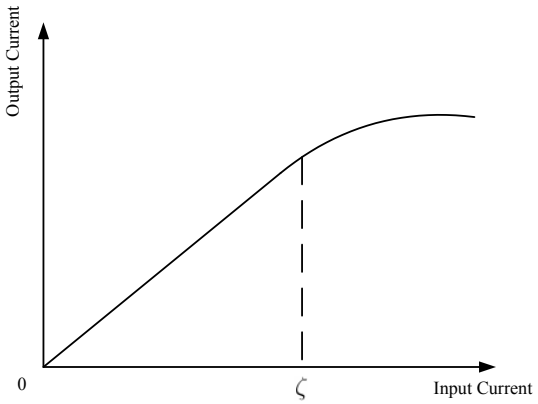

Fig. 3. System impaired by the HPA and LD.

With point-wise non-negative constraints, the waveforms are guaranteed to take non-negative values at the sample points, while they might take slightly negative values at the points in the middle. We thus propose to add an additional small DC bias term after obtaining waveforms designed with the MSM-JDCMP. Simulation results later on show that with $N_O \geq 8$, the negative peak of the designed waveforms is much smaller than the primary DC. Therefore, adding a additional DC does not noticeably cause severe performance loss. With more time samples, the complexity increases while a smaller additional DC is necessary for nonnegative waveforms. There is a tradeoff between the amount of the additional DC and the complexity.

IV. HPA Nonlinear Distortion Mitigation by MSM-JDCMP

In practice, the system encompasses a HPA as in Fig. 2, which may cause nonlinear distortion. Next to HPA, nonlinear distortion is caused by saturation of the output power of the LD. In this paper for illustrative purpose, we only consider the combined effect of these two blocked by studying the associated transfer function $\Gamma(\cdot)$ of the HPA and LD, which can be approximately seen as a linear function for input amplitude smaller than a certain threshold ζ. After the input reaches ζ, $\Gamma(\cdot)$ becomes a nonlinear function as shown by Fig. 3. All sequences $s_i(t)$ contributes to the nonlinear distortion if it falls out of the region $[0, \zeta]$. In this section, we propose to mitigate the nonlinear distortion by our MSM-JDCMP with minimizing the dynamic range, instantaneous PAPR, and long-term PAPR of all possible waveforms as the objective function. With the nonnegative constraint, it is straightforward to observe that the dynamic range is optimized though peak power limitation, i.e, is formulated by (27) or (29). Simulation results for the nonlinear distortion reduction with MSM-JDCMP is shown in Section VI. No single objective is always the best. Depending on particular interests and specific HPA transfer functions, one can choose the most appropriate metric among all, which is beyond the scope of this paper. We only

formulate the optimization problems with the constraints and give simulation results later.

A. The short-term PAPR minimization

- Short-term PAPR: is the ratio of the peak of an individual waveform over its average power. Each individually waveform is constrained under certain PAPR α_i.

The short-term PAPR while symbol $\mathbf{c}_i$ is transmitted is:

$$\check{\Psi}_{e,i}(\mathbf{c_T}) = \frac{(\sum_{k=1}^{K} ||\mathbf{W}_{i,k}\mathbf{c_T}|| + \mathbf{w}_{i,0}^T\mathbf{c_T})^2}{\mathbf{c}_i^T\mathbf{c}_i} = \frac{(\sum_{k=1}^{K} ||\mathbf{W}_{i,k}\mathbf{c_T}|| + \mathbf{w}_{i,0}^T\mathbf{c_T})^2}{\mathbf{c_T}^T\mathbf{J}_i^T\mathbf{J}_i\mathbf{c_T}} \quad (30)$$

$\check{\Psi}_{e,i}(\mathbf{c_T})$ is a convex function of $\mathbf{c_T}$. We seek to minimize the total electrical power under with the short-term PAPR constraint $\check{\Psi}_{e,i}(\mathbf{c_T}) \leq \alpha_i$ ($10\log_{10}\alpha_i$ in dB), we formulate the optimization problem as:

$$\begin{aligned} \min_{\mathbf{c_T}} \quad & \mathbf{c_T}^T\mathbf{c_T} \\ \text{s.t.} \quad & \mathbf{u}_n^T\mathbf{J}_i\mathbf{c_T} \geq 0, \qquad \forall(i,n) \\ & -\mathbf{w}_{i,0}^T\mathbf{c_T} + ||\mathbf{W}_{i,k}\mathbf{c_T}|| - \sqrt{\alpha_i \mathbf{c_T}^T\mathbf{J}_i^T\mathbf{J}_i\mathbf{c_T}} \leq 0, \forall i \\ & 1 - 2\mathbf{c_T}^{(0)T}\mathbf{F}_l\mathbf{c_T} + \mathbf{c_T}^{(0)T}\mathbf{F}_l\mathbf{c_T}^{(0)} \leq 0, \forall l \end{aligned} \quad (31)$$

Linearization is initially done at the point $\mathbf{c_T}^{(0)}$ to yield a convex approximation of the nonconvex PAPR constraint. $\mathbf{c_T}^{(0)}$ is also the starting point of the iterations, which satisfies the nonnegative and minimum distance constraints such that the linearization updates with the iterations.

$$\begin{aligned} \min_{\mathbf{c_T}} \quad & \mathbf{c_T}^T\mathbf{c_T} \\ \text{s.t.} \quad & \mathbf{u}_n^T\mathbf{J}_i\mathbf{c_T} \geq 0, \qquad \forall(i,n) \\ & -\mathbf{w}_{i,0}^T\mathbf{c_T} + ||\mathbf{W}_{i,k}\mathbf{c_T}|| - \sqrt{\alpha_i}[(\mathbf{c_T}^{(0)T}\mathbf{J}_i^T\mathbf{J}_i\mathbf{c_T}^{(0)})^{\frac{1}{2}} - \\ & (\mathbf{c_T}^{(0)T}\mathbf{J}_i^T\mathbf{J}_i\mathbf{c_T}^{(0)})^{-\frac{1}{2}}\mathbf{c_T}^{(0)T}\mathbf{J}_i^T(\mathbf{J}_i\mathbf{c_T} - \mathbf{J}_i\mathbf{c_T}^{(0)})] \leq 0, \forall i \\ & 1 - 2\mathbf{c_T}^{(0)T}\mathbf{F}_l\mathbf{c_T} + \mathbf{c_T}^{(0)T}\mathbf{F}_l\mathbf{c_T}^{(0)} \leq 0, \forall l \end{aligned} \quad (32)$$

B. The long-term PAPR minimization

- Long-term PAPR: is the ratio of the peak of all waveforms over their averaged power, which is assumed to be less than α.

For our scheme, the long-term PAPR is given by:

$$\tilde{\Psi}_e(\mathbf{c_T}) = \frac{\{\max_i(\sum_{k=1}^{K} ||\mathbf{W}_{i,k}\mathbf{c_T}|| + \mathbf{w}_{i,0}^T\mathbf{c_T})\}^2}{\mathbf{c_T}^T\mathbf{c_T}/N_c} = \frac{N_c\{\max_i(\sum_{k=1}^{K} ||\mathbf{W}_{i,k}\mathbf{c_T}|| + \mathbf{w}_{i,0}^T\mathbf{c_T})\}^2}{\mathbf{c_T}^T\mathbf{c_T}} \quad (33)$$

With the long-term PAPR constraint $\tilde{\Psi}_e(\mathbf{c_T}) \leq \alpha$ linearized similarly with the short-term PAPR, the optimization problem can be formulated as:

$$\begin{aligned} \min_{\mathbf{c_T}} \quad & \mathbf{c_T}^T\mathbf{c_T} \\ \text{s.t.} \quad & \mathbf{u}_n^T\mathbf{J}_i\mathbf{c_T} \geq 0, \qquad \forall(i,n) \\ & -\mathbf{w}_{i,0}^T\mathbf{c_T} + ||\mathbf{W}_{i,k}\mathbf{c_T}|| - \sqrt{\frac{\alpha}{N_c}}[(\mathbf{c_T}^{(0)T}\mathbf{c_T}^{(0)})^{\frac{1}{2}} \\ & -(\mathbf{c_T}^{(0)T}\mathbf{c_T}^{(0)})^{-\frac{1}{2}}\mathbf{c_T}^{(0)T}(\mathbf{c_T} - \mathbf{c_T}^{(0)})] \leq 0, \quad \forall i \\ & 1 - 2\mathbf{c_T}^{(0)T}\mathbf{F}_l\mathbf{c_T} + \mathbf{c_T}^{(0)T}\mathbf{F}_l\mathbf{c_T}^{(0)} \leq 0, \qquad \forall l \end{aligned} \quad (34)$$

V. Constellation Labeling

After the optimization problem is solved, we obtain $N_c = 2^{N_b}$ constellation points in a $2K+1$ dimensional space with the minimum Euclidean distance d_{min}. The SER is thus governed by d_{min}. Good constellation labeling scheme, i.e., bit-to-symbol mapping $\mathbf{c}_i = f(\mathbf{b}_i)$, serves to reduce the number of bits in error while the SER is fixed. For smaller constellation sizes, brute force method can be applied to find a global optimal, while for larger constellations the complexity of exhaustive search soon becomes prohibitive. For constellations in high dimensional space as we design, there is no well recognized way of labeling. One heuristic algorithm, termed binary switching algorithm (BSA) by [34] was applied by [32] to output Gray or quasi-Gray mappings for two-dimensional constellations. The BSA can also be applied for labeling constellations in high dimensional space and we show that it significantly outperforms the random mapping.

Denote ξ_d^n as the subset of symbols $\mathbf{c}_i \in \xi$, whose label $\mathbf{b}_i$ has value $d \in \{0,1\}$ in position n, i.e., $\xi_d^n = \{\mathbf{c}_i = f(\mathbf{b}_i),\ \forall \mathbf{b}_i \in \{0,1\}^{N_b} | b_{i,n} = d\}$, $\xi = \{\xi_d^n,\ \forall d \in \{0,1\}, n \in \{1,\cdots,N_b\} \in \mathbb{Z}\}$ (we refer readers to [32, section 2] for details on the definitions), and the cost function to minimize for AWGN channel without prior knowledge can be written as [32, Eq.6]:

$$D^a = \frac{1}{N_b 2^{N_b}} \sum_{n=1}^{N_b} \sum_{d=0}^{1} \sum_{\mathbf{c}_i \in \xi_d^n} \sum_{\hat{\mathbf{c}}_i \in \xi_{\bar{d}}^n} \exp\left(-\frac{|\mathbf{c}_i - \hat{\mathbf{c}}_i|^2}{4N_0}\right) \quad (35)$$

where $\bar{d}$ is the complement of d, i.e., if $d=0$ then $\bar{d}=1$. The BSA iteratively finds a local optimum for a random initial mapping, and several runs are executed to reach the global optimum (details can be found in [32] and references therein). The BSA is shown to greatly outperform random mapping as will be shown in Section VI.

VI. Performance Evaluation

In this section, we assess the power efficiencies and error performances of the MSM-JDCM, MSM-SSPS, and MSM-Normal. Flat-fading channel and rectangular pulse shaping function are assumed through Section VI-A to VI-D and VI-F for illustrative purpose. A practical design example assuming selective-fading channel and TDRC pulse shaping function is considered in Section VI-E. Comparison between MSM and single carrier schemes such as on-off keying (OOK) can be found in [15] and is not included in this paper.

TABLE I
THE POWER GAINS WITH MEDIUM-TO-HIGH SNR.

	$g_{E,16}^{01,22}$	$g_{O,16}^{01,22}$	$g_{P,16}^{01,22}$	$g_{E,16}^{02,22}$	$g_{O,16}^{02,22}$	$g_{P,16}^{02,22}$	$g_{E,16}^{03,22}$	$g_{O,16}^{03,22}$	$g_{P,16}^{03,22}$
$N_b = 4$ (IQ)	0.97	1.08	0.93	3.15	2.28	2.64	4.55	3.36	3.88
$N_b = 4$ (I)	0.58	0.67	0.42				6.27	4.11	3.78
	$g_{E,64}^{01,33}$	$g_{O,64}^{01,33}$	$g_{P,64}^{01,33}$	$g_{E,64}^{02,33}$	$g_{O,64}^{02,33}$	$g_{P,64}^{02,33}$	$g_{E,64}^{03,33}$	$g_{O,64}^{03,33}$	$g_{P,64}^{03,33}$
$N_b = 6$ (IQ)	1.90	1.73	1.06	4.54	2.79	5.98	6.20	4.23	5.54
$N_b = 6$ (I)	1.42	1.21	0.85				7.57	4.70	4.52

A. SER and BER

For the MSM-JDCM and MSM-SPSS, we assume that each symbol is transmitted with equal probability. The union bound of SER is derived as [18, Eq.25]

$$E_{s,1} \approx \frac{2N_n}{N_c} Q\left(\sqrt{\frac{d_{min,1}^2}{2N_0}}\right) \triangleq p_1 Q\left(\sqrt{\frac{d_{min,1}^2}{2N_0}}\right) \tag{36}$$

where $Q(x) = \frac{1}{\sqrt{2\pi}} \int_x^\infty \exp(-t^2/2)dt$ is the Gaussian Q-function, $d_{min,1}$ is the minimum Euclidean distance, and N_n is the number of neighbor pairs (which is defined in Section VI-F). The corresponding BER is

$$E_{b,1} = \frac{\lambda_1}{N_b} E_{s,1} = \frac{\lambda_1}{N_b} p_1 Q\left(\sqrt{\frac{d_{min,1}^2}{2N_0}}\right) \tag{37}$$

where λ_1 denotes the average number of bits in error when one symbol is in error (we seek to minimize λ_1 by the BSA in section VI-F).

For the MSM-Normal, we regard that one symbol is in error if any subcarrier is not correctly detected. The SER can then be derived as

$$\begin{aligned} E_{s,2} &= \tilde{p}_2 \left[1 - \left(1 - Q\left(\sqrt{\frac{d_{min,2}^2}{2N_0}}\right)\right)^K\right] \\ &\approx \tilde{p}_2 K Q\left(\sqrt{\frac{d_{min,2}^2}{2N_0}}\right) \triangleq p_2 Q\left(\sqrt{\frac{d_{min,2}^2}{2N_0}}\right) \end{aligned} \tag{38}$$

where $0 < \tilde{p}_2 < 1$ and $p_2 < p_1$ typically. The approximate equation is valid for medium-to-high SNR case, where the Q-function dominate the SER. The corresponding BER is

$$E_{b,2} = \lambda_2 p_2 Q\left(\sqrt{\frac{d_{min,2}^2}{2N_0}}\right), \qquad \text{for small} \quad N_0 \tag{39}$$

where λ_2 is the average number of bits in error when one symbol is in error.

B. The symbol waveforms and power gains

For the MSM-JDCMP, define the constellations optimized for electrical power, optical power, and peak power with size N_c and K subcarriers as $\Theta_{E,N_c}^{0,K}$, $\Theta_{O,N_c}^{0,K}$, and $\Theta_{P,N_c}^{0,K}$. For the MSM-JDCMB, define the corresponding constellations as $\Theta_{E,N_c}^{1,K}$, $\Theta_{O,N_c}^{1,K}$, and $\Theta_{P,N_c}^{1,K}$. The coordinates of selected optimized constellations are given in Appendix A. Though the MSM-SSPS in [17] is design specifically for reducing the dc-bias, we generalize it to accommodate the electrical power, optical power, and peak power reduction and the corresponding optimized constellations with size N_c are denoted as $\Theta_{E,N_c}^{2,K}$, $\Theta_{O,N_c}^{2,K}$, and $\Theta_{P,N_c}^{2,K}$. For the MSM-Normal, no optimization is associated. $\Theta_{N_c}^{3,K}$ stands for the corresponding constellation with adaptive bias and $\Theta_{N_c}^{4,K}$ for enough-biased[1]. We assume $T_s = 1$ without loss of generality. The oversampling rate $N_O = 8$ without severely adding to computational cost. 300 random initializations are chosen in order to obtain the best constellation. Due to space limit, only the corresponding waveforms with $N_b = 4$ for the three schemes are shown for illustrative purpose.

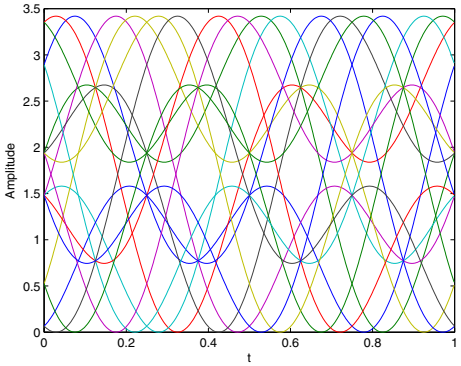

Fig. 4. MSM-normal symbol waveforms with adaptive bias.

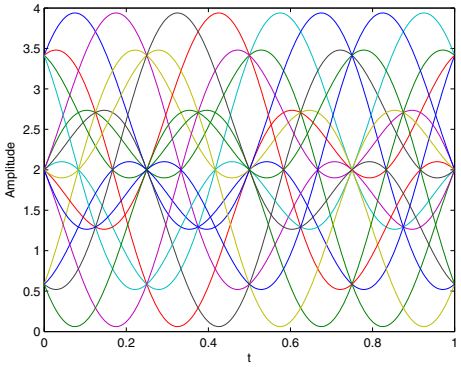

Fig. 5. MSM-normal symbol waveforms with enough bias.

We compare the power efficiencies of the three schemes when *the same target SER and the same spectrum efficiency*

[1]Enough-biased means the DC bias added to each unbiased waveform equals the absolute value of the largest negative peak of all signal waveforms.

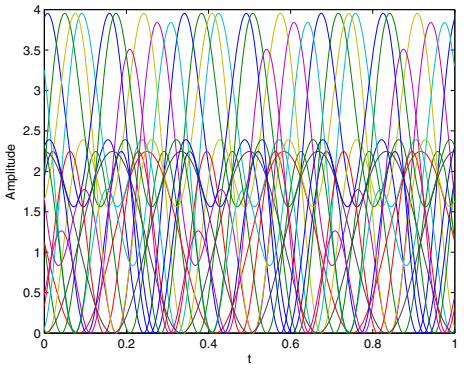

Fig. 6. MSM-SSPS symbol waveforms minimizing the electrical power.

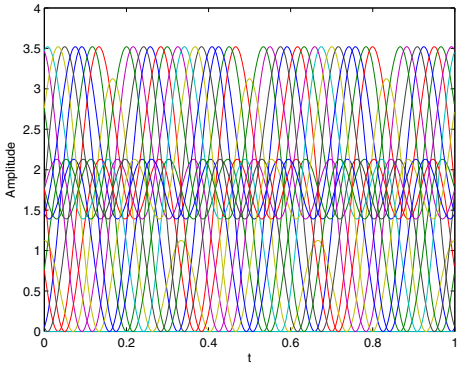

Fig. 7. MSM-SPSS symbol waveforms minimizing the optical power.

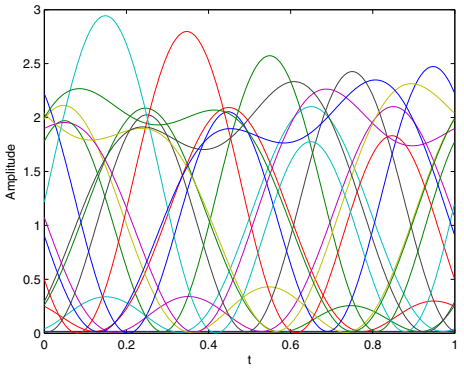

Fig. 8. MSM-JDCMP symbol waveforms minimizing the electrical power.

(bit/s/Hz) are achieved. The power gains are defined as

$$g_{Z,N_c}^{xy,k_xk_y} = 10\log_{10}\frac{P_{Z,N_c}^{y,k_y}}{P_{Z,N_c}^{x,k_x}}\ [\text{dB}] \tag{40}$$

where N_c is the constellation size, $Z \in \{E, O, P\}$, $x, y \in \{0, 1, 2, 3, 4\}$, k_x and k_y are the number of subcarriers scheme x and y use respectively. Since the Q-function part dominate the SERs with medium-to-high SNR, we can neglect the multiplicative factor p_1 and p_2 in this case with only negligible over-estimation of the power gains[2], as in Table I at the bottom of this page.

Fig. 4−Fig. 10 include the designed symbol waveforms accordingly for the MSM-Normal, MSM-SPSS, and MSM-JDCMP with $N_b = 4$ and $K = 2$. Different waveforms

[2]In other words, with medium-to-high SNR, we only need to slightly increase $d_{min,1}$ to obtain a large decrease of SER without significantly increase the overall power.

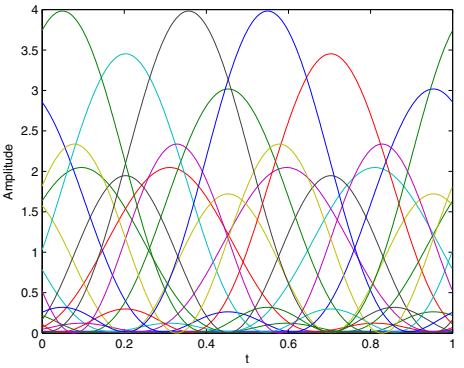

Fig. 9. MSM-JDCMP symbol waveforms minimizing the optical power.

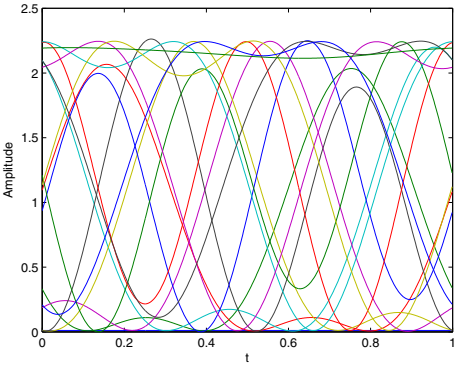

Fig. 10. MSM-JDCMP symbol waveforms minimizing the peak power ($K = 2, N_b = 4$).

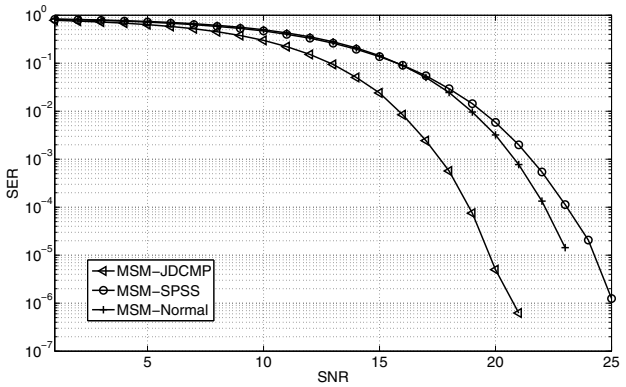

Fig. 11. SER performance of the three schemes when $K = 2$, $N_b = 4$, with the same E_a.

are associated with different colors. We observe that the waveforms associated with the MSM-Normal and MSM-SPSS are less "irregular" while the one with MSM-JDCMP seems more random. Intuitively, the MSM-JDCMP is expected to take better usage of the design space. The Monte-Carlo simulation comparing the symbol error rate performance of the three schemes is shown by Fig. 11, where the testing symbol sequence is of length 2×10^6.

C. Spectral efficiency and Power efficiency tradeoff

Increasing K for a fixed N_b, i.e., sacrificing a portion of the spectrum efficiency, could serve to increase the power efficiency. $\Theta_{E,16}^{0,4}$ offers 2.31dB electrical power gain over $\Theta_{E,16}^{0,2}$. Corresponding waveforms are shown in Fig. 12. It should be noted that no further gain is guaranteed to be achieved with further increasing K, e.g. $\Theta_{E,16}^{0,6}$ is no better

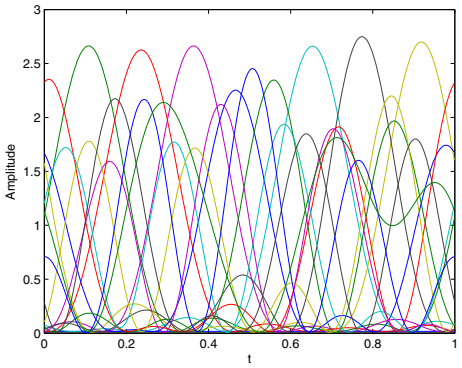

Fig. 12. MSM-JDCMP symbol waveforms minimizing the electrical power ($K = 4, N_b = 4$).

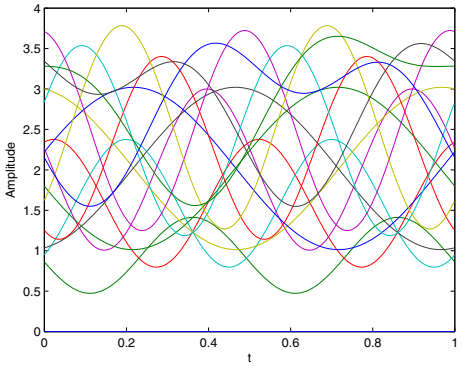

Fig. 13. MSM-JDCMP symbol waveforms with short-term PAPR $\leq$ 3dB.

than $\Theta_{E,16}^{0,4}$.

D. Nonlinear distortion mitigation with the MSM-JDCMP

Fig. 13 shows the waveforms designed to constraint the short-term PAPR to be 3dB with $K = 2$ and $N_b = 4$ by choosing $\alpha_i = \alpha \ \forall i$. Fig. 14 shows the waveforms designed to constraint the long-term PAPR to be 3dB. Whether one criterion is better than the others depends on the exact form of the transfer function of HPA and the probabilities of symbol occurrence. If a certain sequence has a nontrivially higher chance of transmission, it is better to force its amplitude into the linear region and in the mean time control the dynamic range of all sequences.

E. Selective-fading channel with TDRC pulse shaper: a design example

We consider a chosen selective-fading channel

$$h(t) = \frac{1}{2}\delta(t) + \frac{1}{4}\delta(t - \frac{1}{18}) + \frac{1}{10}\delta(t - \frac{1}{9}) + \frac{1}{20}\delta(t - \frac{1}{6}) \quad (41)$$

And we use the window function as defined in (9) as pulse shaper, with the roll-off factor $\beta = 0.1$. When $K = 2$ and $N_b = 4$, we can obtain the pre-equalizer by using Proposition 1 calculated as follows

$$\mathbf{P} = \begin{bmatrix} 1.1111 & 0 & 0 & 0 & 0 \\ 0 & 1.1350 & 0.2620 & 0 & 0 \\ 0 & -0.2620 & 1.1350 & 0 & 0 \\ 0 & 0 & 0 & 1.2230 & 0.5409 \\ 0 & 0 & 0 & -0.5409 & 1.2230 \end{bmatrix} \quad (42)$$

With MSM-JDCMP, the designed waveforms are shown by Fig. 15.

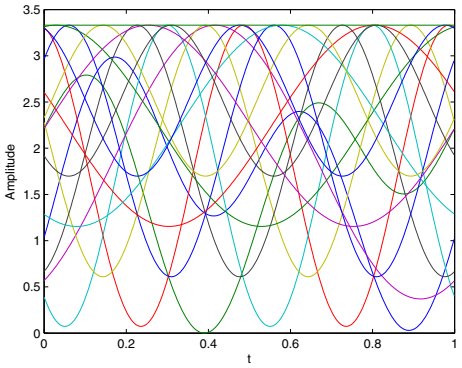

Fig. 14. MSM-JDCMP symbol waveforms with long-term PAPR $\leq$ 3dB.

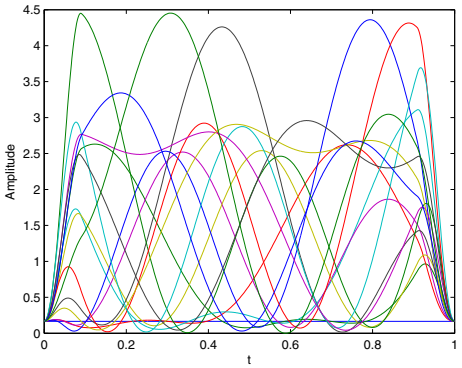

Fig. 15. MSM-JDCMP symbol waveforms minimizing the electrical power with selective-fading channel ($K = 2, N_b = 4$).

F. The improved labelings

Recall the BER in (37)

$$P_b = \frac{2\lambda_1 N_n}{N_b N_c} Q\left(\sqrt{\frac{1}{2N_0}}\right) \quad (43)$$

where the erroneous number of bits λ needs to be minimized. In the previous sections we only calculated the Q function part, while this assumption is only accurate with medium to high SNRs. The constant multiplicative part should also be taken into account with lower SNR.

Two points are treated as neighbors if the following holds

$$1 \leq ||\mathbf{c}_i - \mathbf{c}_j|| \leq 1 + \delta \quad (44)$$

where δ is chosen such that

$$\frac{Q(\sqrt{E_a/2N_0})}{Q(\sqrt{(1+\delta)^2 E_a/2N_0})} \geq \mu \quad (45)$$

$$\text{SNR} = 10\log_{10}\frac{E_a}{N_0} \ [\text{dB}] \quad (46)$$

where SNR stands for the signal-to-noise ratio, E_a is the average electrical energy over all waveforms, μ is a large number so that only pairs with distances smaller than $1 + \delta$ are treated as neighbors, i.e., The pairwise error associated with non-neighbor pairs is neglected. $\mu = 100$ is chosen in this section. It can be observed by simulations that further increasing μ does not change the results much. For $\Theta_{E,16}^{0,2}$, the best corresponding constellation labeling is found for each SNR value by BSA. The exhaustive search method, if applied, needs to compare 64! different labeling such that it is too costly to be useful. It can be observed from Fig. 16 that improved labeling offers a marginal BER gain (0.1dB at 10^{-6}

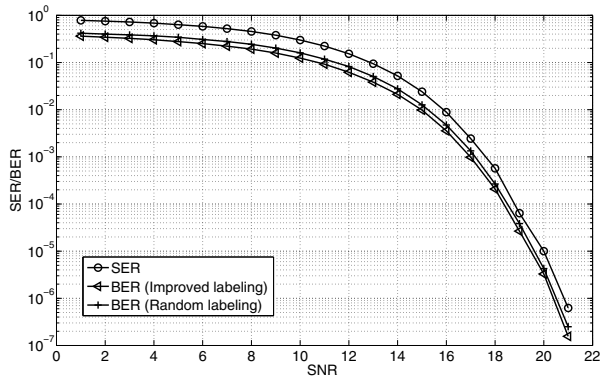

Fig. 16. SER and BER performance with/without improved labeling using MSM-JDCMP to minimize electrical power.

BER) over the random average (over 100 arbitrary trials) labeling ($K = 2, N_b = 4$).

VII. Concluding Remarks

We have proposed a novel and efficient constellation design scheme, termed MSM-JDCM for the optical IM/DD systems. It offers significant power gains over the traditional methods. With the MSM-JDCMP, highly compact sphere packings in higher dimensional space that minimize the electrical/optical/peak powers are found in both flat-fading and selective-fading scenarios. Besides, the MSM-JDCM with PAPR constraints mitigates the system nonlinear distortion. It could potentially be a supplement to many other existing anti-distortion algorithms. In addition, we applied the binary switching algorithm to search for the best labeling. The obtained labeling greatly reduces the BER of the system.

Future directions include: finding tighter bounds to improve the MSM-JDCMB performance and compare with the MSM-JDCMP; study the nonlinear distortion mitigation with a more specific transfer function of the HPA; and analyze effect of channel estimation error on the constellation design.

Appendix A
Selected Optimized Constellations

The optimized constellations $\Theta_{E,16}^{0,2}$, $\Theta_{P,16}^{0,2}$, $\Theta_{E,16}^{1,2}$, and $\Theta_{P,16}^{1,2}$ are listed with a given order $(0000, 0001, \ldots, 1111)$ by applying the BSA at SNR=10dB.

$\Theta_{E,16}^{0,2} = \{(1.4514, 0.0527, 0.6814, 0.3327, 0.0282), (0.7202, 0.5695, 0.1722, 0.3244, 0.2160), (1.2032, 0.2489, 0.3290, -0.2405, 0.7819), (1.1484, -0.2025, -0.0656, 0.6490, 0.4580), (1.4097, 0.6370, 0.1505, -0.1936, -0.2851), (1.1380, 0.1383, -0.0538, 0.6275, -0.4886), (1.4055, 0.3465, -0.5197, 0.0022, 0.3691), (0.7123, 0.3648, -0.5046, -0.1093, -0.3425), (0.7042, 0.0167, 0.6471, -0.3300, 0.0151), (0.7097, -0.6024, 0.1988, 0.2763, -0.2043), (1.4127, -0.6016, 0.1626, -0.1893, 0.3320), (0.7121, -0.3645, -0.5056, -0.1100, 0.3416), (1.1716, -0.1970, 0.2791, -0.2796, -0.7582), (0.0173, 0, 0, 0, 0), (1.1215, 0, -0.1417, -0.7808, -0.0007), (1.4179, -0.3368, -0.5555, -0.0263, -0.3595)\}$

$\Theta_{P,16}^{0,2} = \{(1.4976, 0.3817, 0.6085, 0.1446, -0.3005), (1.5015, -0.3913, 0.5752, 0.1322, 0.3329), (1.0434, -0.0129, 0.1305, -0.7170, -0.1426), (1.5320, -0.6861, -0.1680, -0.2493, -0.1301), (1.4980, 0.7078, -0.1088, -0.3211, 0.1024), (2.1578, 0.0221, 0.0177, 0.0027, -0.0026), (0.7029, 0.3826, 0.5762, -0.1057, 0.2517), (1.1242, 0.0122, -0.1249, -0.1455, 0.6901), (1.1508, -0.0242, -0.1371, 0.0674, -0.6917), (1.1764, -0.0020, 0.0725, 0.7514, 0.0062), (0.7595, -0.5048, 0.5416, -0.0235, -0.3083), (0.7537, -0.6670, -0.2388, 0.2658, 0.2217), (0.7410, 0.6899, -0.1923, 0.2692, -0.1642), (1.5241, 0.1483, -0.7023, 0.2567, 0.1128), (0.0112, 0, 0, 0, 0), (0.6930, 0.0131, -0.6804, -0.2681, -0.0102)\}$

$\Theta_{E,16}^{1,2} = \{(1.6562, -0.4895, 0.2213, 0.5880, 0.2367), (1.0887, -0.2969, 0.7102, 0, 0), (0.8165, 0, 0, -0.0286, -0.5766), (0, 0, 0, 0, 0), (1.3608, 0, 0, 0.0477, 0.9611), (1.0887, 0.6551, 0.4043, 0, 0), (1.6614, 0.1615, 0.5024, 0.0238, -0.6466), (1.6614, -0.5471, -0.2474, 0.5094, 0.1762), (1.0887, -0.7294, -0.2462, 0, 0), (1.6562, -0.4895, 0.2213, -0.5616, 0.2938), (1.0887, 0.1292, -0.7589, 0, 0), (1.3608, 0, 0, 0.8084, -0.5219), (0.8165, 0, 0, -0.4851, 0.3131), (0.8165, 0, 0, 0.5137, 0.2635), (1.6114, 0.5471, -0.2474, -0.4894, 0.2258), (1.3608, 0, 0, -0.8562, -0.4392)\}$

$\Theta_{P,16}^{1,2} = \{(1.6293, 0, 0, -0.9651, -0.6292), (0.8165, 0, 0, 0.4443, 0. - 0.3687), (0.8165, 0, 0, 0.0971, 0.5691), (1.6614, 0.3886, 0.3517, 0.6243, -0.1700), (1.0887, 0.7255, 0.2574, 0, 0), (1.0887, -0.0927, 0.7642, 0, 0), (1.0887, -0.3240, -0.6983, 0, 0), (0, 0, 0, 0, 0), (1.6293, 0, 0, -0.9651, -0.6292), (1.3608, 0, 0, 0.1639, -0.9482), (1.6614, 0.3886, 0.3571, -0.0548, -0.6447), (0.8165, 0, 0, -0.5414, -0.2004), (1.0887, -0.7403, 0.2109, 0, 0), (1.4808, 0.5793, -0.8722, 0, 0), (1.3608, 0, 0, 0.7392, 0.6161), (1.3608, 0, 0, 0.9031, 0.3321)\}$

Appendix B
Proof of Proposition 1

The transmitted signal $s_i(t)$, $i \in [1, N_c]$, can be written as

$$s_i(t) = \eta[m_i(t) + b_i(t)] \qquad t \in [0, T_s] \tag{47}$$

where $m_i(t)$ is an electrical domain waveform before biasing, $b_i(t) = c_{i,0}\Pi(\frac{t}{T_s})$ is the DC-bias. For notation simplicity, we replace $s_i(t)$ and $b_i(t)$ by $s(t)$ and $b(t) = c_0\Pi(\frac{t}{T_s})$. $s(t)$ goes through a frequency selective fading channel defined as in (16), where $\max_i(\tau_i) \ll T_s$ such that $\Pi(\frac{t-\tau_i}{T_s})$ can be approximated by $\Pi(\frac{t}{T_s})$, the receiver-side signal $y(t)$ can be written as

$$\begin{aligned} y(t) &= \gamma\eta[m(t) + b(t)] * h(t) \\ &= \sum_i \beta_i m(t - \tau_i) + c_0 \sum_i \beta_i b(t - \tau_i) \end{aligned} \tag{48}$$

where $\gamma\eta = 1$ is assumed thus the above equation holds. Using basis defined in equation (5)−(8) and with some ma-

nipulations, we have

$$\begin{aligned}\sum_i \beta_i m(t-\tau_i) &\approx \sum_{k=1}^{K}\Big[c_k^c \sum_i \beta_i \cos(2\pi f_k(t-\tau_i)) \\ &\quad + c_k^s \sum_i \beta_i \sin(2\pi f_k(t-\tau_i))\Big]\Pi(\frac{t}{T_s}) \\ &= \sum_{k=1}^{K}\Big[c_k^c \mathrm{Re}\big(\sum_i \beta_i e^{-j2\pi f_k\tau_i}\cdot e^{j2\pi f_k t}\big) \\ &\quad + c_k^s \mathrm{Im}\big(\sum_i \beta_i e^{-j2\pi f_k\tau_i}\cdot e^{j2\pi f_k t}\big)\Big]\Pi(\frac{t}{T_s})\end{aligned} \tag{49}$$

where c_k^c and c_k^s are the real and imaginary part coefficients modulating the k-th basis function. Define $z_k = \sum_i \beta_i e^{-k2\pi f_k\tau_i}$, thus the equation on the bottom of page holds:

In order to compensate the selective fading channel effect, we input c_k^c and c_k^s into the corresponding pre-equalizer which guarantees

$$\begin{cases}\hat{c_k^c}\mathrm{Re}(z_k) + \hat{c_k^s}\mathrm{Im}(z_k) = c_k^c \\ \hat{c_k^s}\mathrm{Re}(z_k) - \hat{c_k^c}\mathrm{Im}(z_k) = c_k^s\end{cases} \tag{50}$$

Therefore

$$\begin{bmatrix}\mathrm{Re}(z_k) & \mathrm{Im}(z_k)\\ -\mathrm{Im}(z_k) & \mathrm{Re}(z_k)\end{bmatrix}\begin{bmatrix}\hat{c_k^c}\\ \hat{c_k^s}\end{bmatrix} = \begin{bmatrix}c_k^c\\ c_k^s\end{bmatrix} \tag{51}$$

$$\begin{bmatrix}\hat{c_k^c}\\ \hat{c_k^s}\end{bmatrix} = \frac{1}{|z_k|^2}\begin{bmatrix}\mathrm{Re}(z_k) & -\mathrm{Im}(z_k)\\ \mathrm{Im}(z_k) & \mathrm{Re}(z_k)\end{bmatrix}\begin{bmatrix}c_j^c\\ c_j^s\end{bmatrix} \triangleq \mathbf{P}_k\begin{bmatrix}c_j^c\\ c_j^s\end{bmatrix} \tag{52}$$

Thus we obtain the pre-equalizers $\mathbf{P}_k$ (k=[1,K]) for each subcarrier. For the biasing part, similarly

$$\sum_i \beta_i b(t-\tau_i) \approx c_0(\sum_i \beta_i)\Pi(\frac{t}{T_s}) \tag{53}$$

therefore, the corresponding pre-equalizer $p_0 = 1/\sum_i \beta_i$.

Remark: The above analysis is based on pulse shape defined by (8). When β is small, the proposition holds approximately when pulse shape given by (9) is used. There are other ways of choosing the pulse-shaping functions, e.g., the cyclic shifted squared root of raised cosine (SRRC) pulse-shaping function suggested in [35]. However, since the complex exponentials are the only eigenfunctions of linear time invariant (LTI) system and use of SRRC will distort the basis, Proposition 1 no longer holds. One might need to design a joint pre-equalizer $\tilde{\mathbf{P}}$ of size $(2K+1)\times(2K+1)$ with non-zero non block-diagonal elements to compensate for both the selective fading channel and change of basis instead of the block diagonal $\mathbf{P}$ suggested in Proposition 1. This is out of the scope of the paper and will be discussed in our future work.

REFERENCES

[1] J. R. Barry, *Wireless Infrared Communications*. Kluwer Academic Press, 1994.

[2] J. M. Kahn and J.R. Barry, "Wireless infrared communications," *Proc. IEEE*, vol. 85, no. 2, pp. 265–298, Feb. 1997.

[3] S. Rajagopal, R. D. Roberts, and S. Lim, "IEEE 802.15.7 visible light communication: modulation schemes and dimming support," *IEEE Commun. Mag.*, Mar. 2012.

[4] Z. Xu and B. M. Sadler, "Ultraviolet communications: potential and state-of-the-art," *IEEE Commun. Mag.*, Mar. 2012.

[5] J. A. C. Bingham, "Multicarrier modulation for data transmission: an idea whose time has come," *IEEE Commun. Mag.*, vol. 28, pp. 5–14, May 1990.

[6] T. E. Darcie, "Subcarrier multiplexing for lightwave networks and video distribution systems," *IEEE J. Sel. Areas Commun.*, vol. 8, pp. 1240–1248, Sept. 1990.

[7] J. B. Carruthers and J. M. Kahn, "Multiple-subcarrier modulation for nondirected wireless infrared communication," *IEEE J. Sel. Areas Commun.*, vol. 14, no. 3, pp. 538–546, Apr. 1996.

[8] J. Armstrong, "OFDM for optical communications," *J. Lightw. Technol.*, vol. 27, no. 3, pp. 189–204, Feb. 2009.

[9] O. Gonzales, "OFDM over indoor wireless optical channel," *IEE Proc. Optoelectron.*, vol. 152, no. 4, pp. 199–204, Aug. 2005.

[10] S. Hranilovic and S. Kumar, "All-optical multihop free-space optical communication systems," *J. Lightw. Technol.*, vol. 29, no. 18, pp. 2663–2669, Sept. 2009.

[11] N. Cvijetic and T. Wang, "WiMAX over free-space optics—evaluating OFDM multi-subcarrier modulation in optical wireless channels," *2006 IEEE Sarnoff Symposium.*

[12] A. S. Lioumpas, G. K. Karagiannidis, and S. Arnon, "Adaptive subcarrier PSK intensity modulation in free space optical systems," *IEEE Trans. Commun.*, vol. 59, no. 5 pp. 1368–1377, May 2011.

[13] M. Z. Hassan, "Subcarrier intensity modulated wireless optical communications with rectangular QAM," *J. Opt. Commun. Netw.*, vol. 4, no. 6, pp. 522–532, June 2012.

[14] W. O. Popoola, "Subcarrier intensity modulated free-space optical communication systems," Ph.D. thesis, Northumbria University, 2009.

[15] R. You and J. Kahn, "Average power reduction techniques for multiple-subcarriers intensity-modulated optical signals," *IEEE Trans. Commun.*, vol. 49, no. 12, pp. 2164–2170, Dec. 2001.

[16] T. Ohtsuki, "Multiple-subcarrier modulation in optical wireless communications," *IEEE Commun. Mag.*, vol. 41, no. 3, pp. 74–79, Mar. 2003.

[17] S. Teramoto and T. Ohtsuki, "Multiple-subcarrier optical communication systems with subcarrier signal-point sequence," *IEEE Trans. Commun.*, vol. 53, no. 10, pp. 1738–1743, Oct. 2005.

[18] J. Karout, E. Agrell, K. Szczerba, and M. Karlsson, "Optimizing constellations for single-subcarrier intensity modulated optical systems," *IEEE Trans. Inf. Theory*, vol. 58, no. 7, pp. 4645–4659, July 2012.

[19] Q. Gao, J. H. Manton, G. Chen, and Y. Hua, "Power-efficient constellation design for a multicarrier optical wireless system," in *Proc. 2013 IEEE Milcom*, pp. 1645–1650.

[20] cvx Users' Guide, CVX Research, Inc.

[21] H. Chen and H. Liang, "Combined selective mapping and binary cyclic codes for PAPR reduction in OFDM systems," *IEEE Trans. Wireless Commun.*, vol. 6, no. 10, pp. 3524–3528, Oct. 2007.

[22] S. H. Muller and J. B. Huber, "OFDM with reduced peak-to-average power ratio by optimum combination of partial transmit sequences," *IEE Electron. Lett.*, vol. 33, pp. 368–369, Feb. 1997.

[23] Y. Wang and Z. Luo, "Optimized iterative clipping and filtering for PAPR reduction of OFDM signals," *IEEE Trans. Commun.*, vol. 59, no. 1, pp. 33–37, Jan. 2001.

[24] J. Chen and C. Li, "Tone reservation using near-optimal peak reduction tone set selection algorithm for PAPR reduction in OFDM systems," *IEEE Signal Process. Lett.*, vol. 17, no. 11, pp. 933–936, Nov. 2010.

$$\begin{aligned}\sum_i \beta_i m(t-\tau_i) &\approx \sum_{k=1}^{K}\Big[c_k^c \sum_i \beta_i \cos(2\pi f_k(t-\tau_i)) + c_k^s \sum_i \beta_i \sin(2\pi f_k(t-\tau_i))\Big]\Pi(\frac{t}{T_s}) \\ &= \sum_{k=1}^{K}\Big[c_k^c \mathrm{Re}\big(\sum_i \beta_i e^{-j2\pi f_k\tau_i}\cdot e^{j2\pi f_k t}\big) + c_k^s \mathrm{Im}\big(\sum_i \beta_i e^{-j2\pi f_k\tau_i}\cdot e^{j2\pi f_k t}\big)\Big]\Pi(\frac{t}{T_s})\end{aligned}$$

[25] F. Boccardi and G. Caire, "The p-sphere encoder: peak-power reduction by lattice precoding for the MIMO Gaussian broadcast channel," *IEEE Trans. Commun.*, vol. 54, no. 11, pp. 2085–2091, Nov. 2006.
[26] T. Jiang, Y. Yang, and Y. Song, "Exponential companding transform for PAPR reduction in OFDM systems," *IEEE Trans. Broadcast.*, vol. 51, no. 2, pp. 244–248, June 2005.
[27] S. Han and J. Lee, "An overview of peak-to-average power ratio reduction techniques for multicarrier transmission," *IEEE Trans. Wireless Commun.*, vol. 9, no. 2, pp. 523–527, Apr. 2005.
[28] F. Gray, "Pulse code communications," U.S. Patent 2 632 058, Mar. 1953.
[29] G. Ungerboeck, "Channel coding with multilevel/phase signals," *IEEE Trans. Inf. Theory*, vol. 28, no. 1, pp. 55–67, Jan. 1982.
[30] G. Ungerboeck, "Trellis-coded modulation with redundant signal sets—parts I and II," *IEEE Commun. Mag.*, vol. 25, pp. 5–20, Feb. 1987.
[31] J. Tan and G. Stuber, "Analysis and design of symbol mappers for iteratively decoded BICM," *IEEE Trans. Wireless Commun.*, vol. 4, no. 2, Mar. 2005.
[32] F. Schreckenbach, N. Gortz, J. Hagenauer, and G. Bauch, "Optimization of symbol mappings for bit-interleaved coded modulation with iterative decoding," *IEEE Commun. Lett.*, vol. 7, no. 12, Dec. 2003.
[33] M. Beko and R. Dinis, "Designing good multi-dimensional constellations," *IEEE Wireless Commun. Lett.*, vol. 1, no. 3, pp. 221–224, June 2012.
[34] K. Zeger and A. Gersho, "Pseudo-gray coding," *IEEE Trans. Commun.*, vol. 38, pp. 2147–2158, Dec. 1990.
[35] S. B. Slimane, "Peak-to-average power ratio reduction of OFDM signals using broadband pulse shaping," in *Proc. 2002 IEEE VTC*, vol. 2, pp. 889–893.
[36] J. B. Carruthers and J. M. Kahn, "Modeling of nondirected wireless infrared channels," *IEEE Trans. Commun.*, vol. 45, no. 10, Oct. 1997.

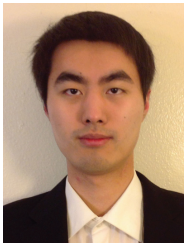

Qian Gao was born in Shandong, China, in 1987. He received the B.E. degree from Nanjing University of Science and Technology, China, in 2009 and the M.Sc. degree from University of California at Riverside (UCR), USA, in 2010, from where he is now pursuing the Ph.D. degree. His research interests include signal processing in radio frequency, visible light communication and ultraviolet communication networks, statistical and array signal processing, applications of linear algebra and optimization methods, and advanced modulation design for optical multiple-color multiple-carrier systems. He is currently members of IEEE, SPIE, and OSA.

Jonathan Manton holds a distinguished Chair at the University of Melbourne with the title Future Generation Professor. He is also an Adjunct Professor in the Mathematical Sciences Institute at the Australian National University. He received his Bachelor of Science (mathematics) and Bachelor of Engineering (electrical) degrees in 1995 and his Ph.D. degree in 1998, all from the University of Melbourne, Australia. From 1998 to 2004, he was with the Department of Electrical and Electronic Engineering at the University of Melbourne. During that time, he held a Postdoctoral Research Fellowship then subsequently a Queen Elizabeth II Fellowship, both from the Australian Research Council. In 2005 he became a full Professor in the Department of Information Engineering, Research School of Information Sciences and Engineering (RSISE) at the Australian National University. From July 2006 till May 2008, he was on secondment to the Australian Research Council as Executive Director, Mathematics, Information and Communication Sciences.

Manton's traditional research interests range from pure mathematics (e.g. commutative algebra, algebraic geometry, differential geometry) to engineering (e.g. signal processing, wireless communications). He has recently served as a Guest Editor for a special issue on Differential Geometry in Signal Processing, he has been an Associate Editor for IEEE TRANSACTIONS ON SIGNAL PROCESSING and Committee Member for IEEE Signal Processing for Communications (SPCOM) Technical Committee.

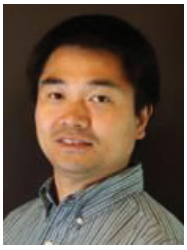

Gang Chen received Ph.D. degree in optical engineering from Shanghai Institute of Optics and Fine Mechanics, CAS, China, in 2004. From 1997 to 2006, he was an Assistant Professor then an Associate Professor at Shanghai Institute of Optics and Fine Mechanics, CAS, focusing on free space ultraviolet and infrared communications, optical fiber communication and sensing. Since 2006, he has been a postdoctoral scholar in the Department of Electrical Engineering, University of California at Riverside (UCR). From 2011, he was promoted to an Associate Adjunct Professor at UCR. His current research interests lie in wireless optical communications and sensing system design. Dr. Chen is a Member of SPIE and IEEE.

Yingbo Hua (S'86–M'88–SM'92–F'02) received a B.S. degree (1982) from Southeast University, Nanjing, China, a M.S. degree (1983) and a Ph.D. degree (1988) from Syracuse University, Syracuse, NY. He was a Lecturer (1990-1992), a Senior Lecturer (1993-1995), and a Reader and Associate Professor (1996-2000) with the University of Melbourne, Australia. He was a Visiting Faculty Member with Hong Kong University of Science and Technology (1999-2000), and a Consultant with Microsoft Research, WA (summer 2000). Since 2001, he has been with the University of California at Riverside, where he is a Senior Full Professor.

Dr. Hua has served as Editor, Guest Editor, Member of Editorial Board and/or Member of Steering Committee for IEEE TRANSACTIONS ON SIGNAL PROCESSING, IEEE SIGNAL PROCESSING LETTERS, *EURASIP Signal Processing*, *IEEE Signal Processing Magazine*, IEEE JOURNAL ON SELECTED AREAS IN COMMUNICATIONS, and IEEE WIRELESS COMMUNICATION LETTERS. He has been a Member of IEEE Signal Processing Society's Technical Committees for Underwater Acoustic Signal Processing, Sensor Array and Multichannel Signal Processing, and Signal Processing for Communication and Networking. He has served as member of Technical and/or Advisory Committees for over forty international conferences and workshops. He has authored over three hundreds of articles and coedited three volumes of books, with more than six thousands of citations, in the fields of Sensing, Signal Processing and Communications. He is a Fellow of IEEE and AAAS.